Analyst

ROYAL SOCIETY OF CHEMISTRY

PAPER

View Article Online
View Journal | View Issue

Cite this: *Analyst*, 2024, **149**, 2436

A disposable paper-based electrochemical biosensor decorated by electrospun cellulose acetate nanofibers for highly sensitive bio-detection†

Zhiwei Zhang,‡[a] Manman Du,‡[a,b] Xiao Cheng,‡[a] Xuechen Dou,[a] Junting Zhou,[a,c] Jianguo Wu,[a,c] Xinwu Xie *[a,d] and Mengfu Zhu*[a,d]

Paper-based electrochemical sensors have the characteristics of flexibility, biocompatibility, environmental protection, low cost, wide availability, and hydropathy, which make them very suitable for the development and application of biological detection. This work proposes electrospun cellulose acetate nanofiber (CA NF)-decorated paper-based screen-printed (PBSP) electrode electrochemical sensors. The CA NFs were directly collected on the PBSP electrode through an electrospinning technique at an optimized voltage of 16 kV for 10 min. The sensor was functionalized with different bio-sensitive materials for detecting different targets, and its sensing capability was evaluated by CV, DPV, and chronoamperometry methods. The test results demonstrated that the CA NFs enhanced the detection sensitivity of the PBSP electrode, and the sensor showed good stability, repeatability, and specificity ($p < 0.01$, $N = 3$). The electrochemical sensing of the CA NF-decorated PBSP electrode exhibited a short detection duration of ~5–7 min and detection ranges of 1 nmol mL^{-1}–100 μmol mL^{-1}, 100 fg mL^{-1}–10 μg mL^{-1}, and 1.5 × 10^{2}–10^{6} CFU mL^{-1} and limits of detection of 0.71 nmol mL^{-1}, 89.1 fg mL^{-1}, and 30 CFU mL^{-1} for glucose, Ag85B protein, and *E. coli O157:H7*, respectively. These CA NF-decorated PBSP sensors can be used as a general electrochemical tool to detect, for example, organic substances, proteins, and bacteria, which are expected to achieve point-of-care testing of pathogenic microorganisms and have wide application prospects in biomedicine, clinical diagnosis, environmental monitoring, and food safety.

Received 31st January 2024,
Accepted 4th March 2024

DOI: 10.1039/d4an00164h

rsc.li/analyst

1 Introduction

Pathogens are infectious agents that cause disease, including viruses, bacteria, fungi, *etc*. Pathogens enter the body through a variety of infections and cause more than 15 million deaths worldwide each year.[1] For example, tuberculosis (TB) is a chronic infectious disease caused by *Mycobacterium tuberculosis* (MTB) and is mainly spread through the respiratory tract. TB has high morbidity and mortality and is one of the top ten causes of death in low- and middle-income countries around the world. Ag85B protein is the main secreted protein of MTB, which can be obtained without cell rupture and has high application potential in the clinical diagnosis of TB.[2] *Escherichia coli* (*E. coli*) is a bacterium that normally inhabits the intestines of humans and animals. *E. coli O157:H7* is a major pathogenic bacterium among hemorrhagic *E. coli* and is mainly spread through water and food, causing environmental pollution and food safety problems.[3] Diabetes is a metabolic disease characterized by hyperglycemia and is a common and frequently-occurring disease. Glucose is one of the important detection indicators of diabetes.[4] Therefore, the point-of-care testing (POCT) of pathogenic microorganisms is of great significance in the fields of biomedicine, clinical diagnosis, environmental monitoring, and food safety.[5–8]

Electrochemical sensors have the advantages of a short detection time (5–10 min), high sensitivity, high anti-interference resistance, simple operation, and low cost and have the potential to realize the rapid on-site detection of pathogenic microorganisms.[1,9–12] Recently, electrochemical sensors based on different materials have been widely used, among which paper-based electrochemical sensors have become

[a]*Systems Engineering Institute, People's Liberation Army, Tianjin 300161, China. E-mail: xinwuxie@163.com, zmf323@163.com; Fax: +86-022-84660562; Tel: +86-022-84660562*
[b]*School of Environmental Science and Engineering, Tianjin University, Tianjin, 300072, China*
[c]*School of Electronic Information and Automation, Tianjin University of Science and Technology, Tianjin 300222, China*
[d]*National Bio-Protection Engineering Center, Tianjin 300161, China*

†Electronic supplementary information (ESI) available. See DOI: https://doi.org/10.1039/d4an00164h

‡These authors contributed equally to this work.

research hotspots due to their flexibility, biocompatibility, environmental protection, low cost, wide availability, and hydrophilic properties.[13] However, for electrochemical biosensors, there remains room for improvement in obtaining high sensitivity, selectivity, specificity, and a low limit of detection (LOD) of detection results in a short time.[14,15]

In the detection studies of electrochemical biosensors, biomolecules to be identified are usually fixed onto the surface of the sensor detection electrode.[16] The materials that fix the biological receptors have an impact on the sensing characteristics of the biosensors, such as the linear detection range, LOD, and sensitivity. The immobilized support material must not only immobilize the biomolecules onto the sensor surface, but also maintain its function during the detection process, and it must not affect the diffusion of the sample.[17] Although the surface of paper-based electrochemical sensors can easily be chemically and physically modified, cut, folded, and stacked, their specific surface area remains an important parameter to increase detection sensitivity.[18] Thus, nanotechnologies and nanomaterials can play a key role in the fixation of biomolecules on the electrode surface.[19] Among various nanomaterials, nanofibers (NFs) prepared by electrospinning technology have the advantages of large surface areas and easy functionalization, which are conducive to the immobilization of biomolecules.[20] Because of these important features, studies of nanofiber membranes of various materials have been used as platforms for fixing biological receptors. These platforms have been used to immobilize enzymes,[21] antibodies,[22] aptamers,[23] whole cells,[24] and synthetic molecularly imprinted polymers[25] for the development of electrochemical biosensing.

As an organic polymer, cellulose acetate (CA) is biocompatible, inexpensive, and thermally and chemically stable and has a high binding affinity with other substances. Therefore, cellulose acetate nanofibers (CA NFs) offer numerous advantages, in which the high specific surface area and the high interconnectivity are associated with the sensing properties of the sensor.[26] These properties of CA NFs allow for various biomedical applications, namely, in biosensors that act as a structure for the immobilization of biomolecules.[27] These fibers have more binding and capture capabilities because of their own interconnected three-dimensional structure and are better fixed biomolecules (antibodies, DNA, and enzymes) for the detection of different analytes, such as organic compounds,[28] bacteria,[29] and cancer biomarkers,[30] respectively. Li *et al.* prepared biosensors for glucose detection by encapsulating enzymes into the metal–organic frameworks and anchoring them to the nanofiber membrane.[21] Zhai *et al.* prepared an electrochemical sensor based on CA NF membranes to detect ascorbic acid by cyclic voltammetry (CV).[31] Ahmadi *et al.* proposed an rGO modification electrochemical sensor-based regenerated cellulose nanofiber that enables the detection of glucose (3.3–27.7 mM).[32] Fakude *et al.* prepared carbon nanofiber dispersions that were immobilized on the streptavidin-modified sensor surface to enable the detection of cadmium (II).[33] However, the preparation of electrochemical biosensors with low cost, high sensitivity, selectivity, specificity, and simple operation remains challenging.

In this study, a simple, inexpensive, and disposable electrochemical biosensor was proposed. First, electrospun CA NFs were directly collected on a paper-based screen-printed (PBSP) electrode using an electrospinning technique. The biomolecules were then immobilized on the CA NF-decorated PBSP electrode. The sensor was modified with glucose oxidase (GOD), Ag85B antibody, and *E. coli O157:H7* monoclonal antibodies to detect glucose, Ag85B protein, and *E. coli O157:H7*, respectively. Typical electrochemical analytical methods such as CV, DPV, and chronoamperometry were used for the sensing and the results were compared with those of bare electrodes. The CA NF-decorated PBSP biosensor demonstrated good performance in all tests. The electrospun CA NF-decorated PBSP electrochemical biosensors have wide application prospects in biomedicine, clinical diagnosis, environmental monitoring, and food safety.

2 Materials and methods

2.1 Reagents and materials

Cellulose acetate (CAS 9004-35-7) with a molecular weight of 30 000 was procured from Sigma Aldrich (Missouri, USA). *N*,*N*-Dimethylacetamide (DMAc, CAS 127-19-5) was procured from Aladdin (Shanghai, China). 0.1 M phosphate buffered saline (PBS) and glucose (CAS 50-99-7) were purchased from Solarbio (Beijing, China). The bacteria used in this study (*E. coli O157: H7*, *E. coli ATCC8099*, and *Bacillus subtilis ATCC9372*) were provided by the China Center of Industrial Culture Collection (Beijing, China). GOD was purchased from Aladdin (Shanghai, China). Ag85B protein and anti-Ag85B antibodies were purchased from Abcam (JHY, UK). The 5 wt% Nafion perfluorinated resin solution (CAS 31175-20-9) was purchased from MACKLIN (Shanghai, China). Potassium ferrocyanide ($K_4Fe(CN)_6$, CAS 13746-66-2) and potassium ferricyanide ($K_3Fe(CN)_6$, CAS 13943-58-3) were purchased from Kaitong (Tianjin, China). 3-(3-Dimethylaminopropyl)-1-ethylcarbodiimide hydrochloride (EDC, CAS 25952-53-8) and *N*-hydroxysuccinimide (NHS, CAS 6066-82-6) were procured from Adamas-beta (Shanghai, China).

The culture process of *E. coli O157: H7*, *E. coli ATCC8099*, and *Bacillus subtilis ATCC9372* is referred to in our previous research.[34] Then, the cultured bacteria were suspended in PBS and diluted to an optimal concentration of approximately 10^{10} CFU mL^{-1}.

Fig. 1a shows the schematic of electrochemical biosensor detection, including the electrochemical chip, detecting instrument, and computer software. The PBSP electrodes, the core part of the electrochemical chip, were processed using POTEN (Shandong, China). The working and counter electrodes were made of carbon and the reference electrode was made of Ag/AgCl. The working electrodes had a diameter of 4 mm. The thickness of the electrode was 0.3 mm. The working, reference, and counter electrodes were integrated into the paper sub-

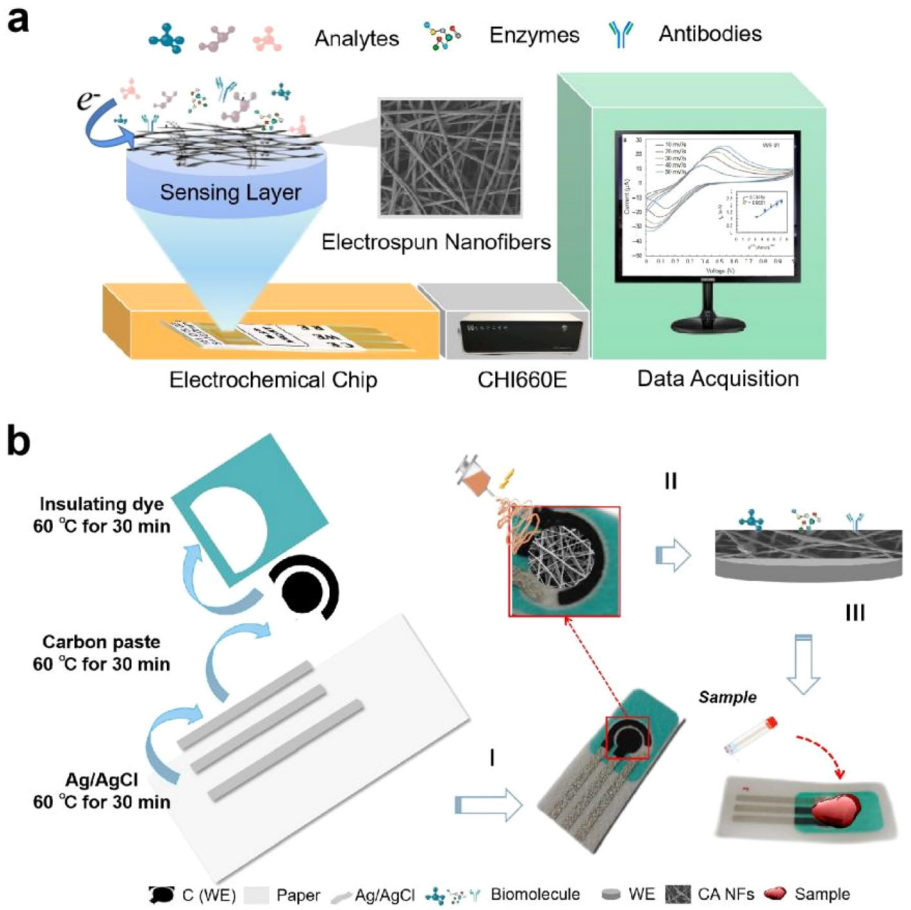

Fig. 1 (a) Schematic of electrochemical biosensor devices based on electrospun nanofibers and (b) the preparation process of the CA NF-decorated PBSP electrode.

strate using screen-printing technology. Screen-printing templates and printing inks are vital to the manufacturing process. Graphite, Ag/AgCl templates, and insulation templates were designed using CAD, and the corresponding ink was printed layer-by-layer on the paper substrate. Silver wires connected to the electrodes were printed on a paper-based substrate. The electrode surface was also covered with an insulating layer (Fig. 1b).

2.2 Fabrication of CA NFs using the electrospinning technique

The CA nanofibers were prepared using electrostatic spinning equipment (TL-Pro, TONGLI, Shenzhen, China). CA NFs were prepared based on voltage (11, 16, and 21 kV) at a fixed concentration of CA solution (11 wt%). First, the CA powder and solvent were continuously stirred at 200 rpm at 25–80 °C at a ratio of 1 : 10, where the solvent was prepared from acetone and DMAc in a 2 : 1 ratio. Then, the CA solution was loaded into a 20 mL syringe, where the syringe was fitted with an internal diameter of 0.7 mm metal needle, and the syringe was connected to a sliding table (tip-to-collector distance = 15 cm, flow rate = 0.5 mL h^{-1}). The CA NFs were collected directly on the PBSP electrode (Fig. 1b). Fig. S1† shows the schematic of the electrospinning device. After drying the CA NF-decorated PBSP electrodes with nitrogen for 10 s, the CA NFs were treated with a 5 wt% Nafion solution (5 μL) to improve adhesion. The CA NF-decorated PBSP electrodes were used for biomolecule (GOD, Ag85B antibody, and *E. coli O157:H7* monoclonal antibody) immobilization.

2.3 Biomolecule immobilization on the CA NF-decorated PBSP electrode

First, EDC (19.17 mg) and NHS (2.1712 mg) were dissolved in 1 mL PBS at room temperature. Next, 10 μL of the mixed solution was dripped onto the working electrode surface (CA NF-decorated PBSP electrode) and kept for 2 h at room temperature. Subsequently, the CA NF-decorated PBSP electrode surface was washed carefully with DI water 3–4 times and blow-dried with nitrogen after cleaning. Different concentrations of biomolecular suspensions (GOD, Ag85B antibody, and *E. coli O157:H7* monoclonal antibody) were prepared, and samples (10 μL each) were added to the surface of the working electrode for detection.

2.4 Characterization techniques

The morphology and diameter of the bare PBSP electrodes and CA NF-decorated and GOD /CA NF-decorated PBSP electrodes were observed using a scanning electron microscope (SEM) and a ZEISS Sigma 300 instrument. To investigate the various functional groups and chemical bonds present in the process of fixing biomolecules on the surface of the CA-decorated PBSP electrodes, Fourier-transform infrared spectroscopy (FT-IR) was performed using a DTGS KBr instrument. The sensor was tested by CHI600E using the electrochemical impedance spectroscopy (EIS) method to investigate the surface-modified electrodes at the open circuit potential by applying an amplitude of 5 mV within the frequency range from 1 to 10^5 Hz.

2.5 Detection of bioagents

For the optimization of the electrospinning parameters, the electrochemical sensing of the fabricated CA NF-decorated PBSP electrode with 100 U of GOD was recorded using differential pulse voltammetry (DPV) in PBS containing 50 mM $[Fe(CN)_6]^{3-/4-}$ at a scan rate of 50 mV s^{-1} in the potential range from −1 to 1 V. The results were compared using electrospinning at 11, 16, and 21 V for 10 min with modified GOD in 1 μmol mL^{-1} glucose solution. At a voltage of 16 kV, electrospinning was conducted for 5, 10, and 15 min with modified GOD in 1 μmol mL^{-1} of glucose solution, and the test results were compared.

For the detection of glucose, the electrochemical sensing of the fabricated CA NF-decorated PBSP electrode with 100 U GOD was recorded using CV and DPV in PBS containing 50 mM $[Fe(CN)_6]^{3-/4-}$ at a scan rate of 50 mV s^{-1} in the potential range from −1 to 1 V. The glucose is oxidized to gluconolactone under the catalysis of GOD. $[Fe(CN)_6]^{3-/4-}$ in PBS facilitates the electron-transfer reaction. Seven concentration gradients of glucose were tested (control, 1, 10, 100, 10^3, 10^4, and 10^5 nmol mL^{-1}).

For the detection of Ag85B protein, the electrochemical response of the CA NF-decorated PBSP electrode to Ag85B protein was determined at different concentrations (0.1, 1, 10, 100, 10^3, and 10^4 ng mL^{-1}). Specific binding reactions of the Ag85B protein occur with the Ag85B antibody. Detection was performed by chronoamperometry to ensure the completion of the Ag85B antibody–Ag85B protein interaction. The results were recorded for 400 s at approximately −0.15 V with pulses every 0.1 s.

For the detection of *E. coli O157:H7*, the electrochemical response of the CA NF-decorated PBSP electrode to *E. coli O157:H7* was determined at different concentrations (1.5×10, 1.5×10^2, 1.5×10^3, 1.5×10^4, 1.5×10^5, and 1.5×10^6). Specific binding reactions of *E. coli O157:H7* occur with the *E. coli O157:H7* monoclonal antibody. Chronoamperometry was recorded for 400 s. Specific detection experiments were performed using sensors modifying the *E. coli O157:H7* monoclonal antibody against *E. coli O157:H7*, *E. coli ATCC8099*, and *Bacillus subtilis ATCC9372* at concentrations of 1.5×10^5 CFU mL^{-1}.

3 Results and discussion

3.1 Optimization of electrospinning parameters

To improve the performance after coating, we optimized the parameters of the electrospinning techniques. Fig. 2a shows the SEM images of the CA NFs at different voltages. The diameters of the NFs at different voltages were calculated as 463.52 ± 251.76 nm, 270.13 ± 46.93 nm, and 460.97 ± 208.88 nm (Fig. 2b). Fig. 2c shows the signal values of glucose detection (1 μmol mL^{-1}) when the electrodes are coated by electrospinning at 11, 16, and 21 kV for 10 min (2.28 ± 0.38, 15.55 ± 0.96, and 8.43 ± 2.17, $p < 0.01$) and modified by GOD. The NFs fabricated using a voltage of 16 kV had a smaller size and better uniformity than the other voltage (DPV curves in Fig. S2†), which produces more pores, a larger specific surface area, and more sites for biomolecule binding; thus, the CA NF-decorated PBSP electrode has a higher electric response and better detection capacity than the PBSP electrode. Based on these results, 16 kV was used for further electrospinning. The electrospinning duration (5, 10, and 15 min) was optimized (Fig. 2d, DPV curves in Fig. S3†). Fig. S4† shows the SEM images of the cross-section and the thickness of the CA NFs at different electrospinning durations. These results indicate that the 10 min group had a significantly higher response rate than the other groups. Therefore, 10 min were used for further electrospinning.

3.2 Characterization of the surface modification process of the electrode

SEM images of the bare PBSP electrodes and CA NF-decorated PBSP electrodes are shown in Fig. 3a and b, respectively. Fig. 3b shows that the distribution of the CA NFs is mostly uniform and forms a polymer network of the NFs. According to the SEM results, the CA NF-decorated PBSP electrode had a porous surface morphology and an interconnected network structure. The presence of its network structure increases the specific surface area and provides a good platform for biomolecule immobilization (Fig. 3b). The SEM image revealed that the surface morphology of the NF network changed slightly after fixing the GOD (Fig. 3c). These results illustrated that the biomolecules were successfully immobilized on the surface of the CA NF-decorated PBSP electrode.

In addition, we employed EIS to characterize bare electrodes, CA NF-decorated electrodes, and CA NF-decorated electrodes with GOD. The Nyquist plots of the different electrodes in the frequency range of 1–10^5 Hz are shown in Fig. 3d. Since CA NFs themselves are not conductive, covering the surface of the PBSP electrodes with CA NFs reduces the conductivity of the detected area, showing a larger semicircle in the Nyquist plot. Due to the high porosity of CA NFs, they also have an embedding rate.[35] When the biomolecules were immobilized on the surface of CA NF-decorated PBSP electrodes, the redox centers of some bioactive substances would be buried in the three-dimensional space structure of CA NFs, resulting in slower electron transfer speed and increased impedance. The FT-IR spectra of the CA NF-decorated PBSP electrodes are shown in

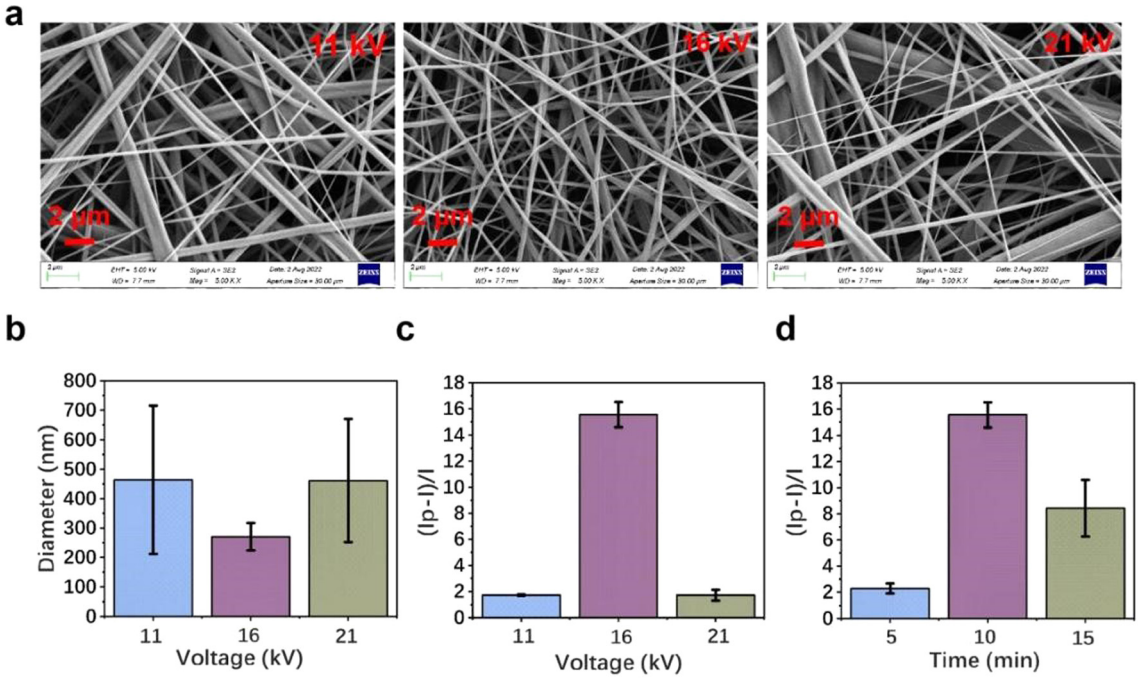

Fig. 2 Optimization of electrospinning conditions. (a) SEM images at different voltages; (b) average diameter distribution at different voltages; and (c) glucose (1 μmol mL^{-1}) detection responses of electrospinning CA NFs at different voltages (11, 16, and 21 kV, electrospinning duration = 10 min); (d) glucose (1 μmol mL^{-1}) detection responses of electrospinning CA NFs at different electrospinning durations (5, 10, and 15 min, voltage = 16 kV). (*Ip*: value of peak current, *I*: value of base current).

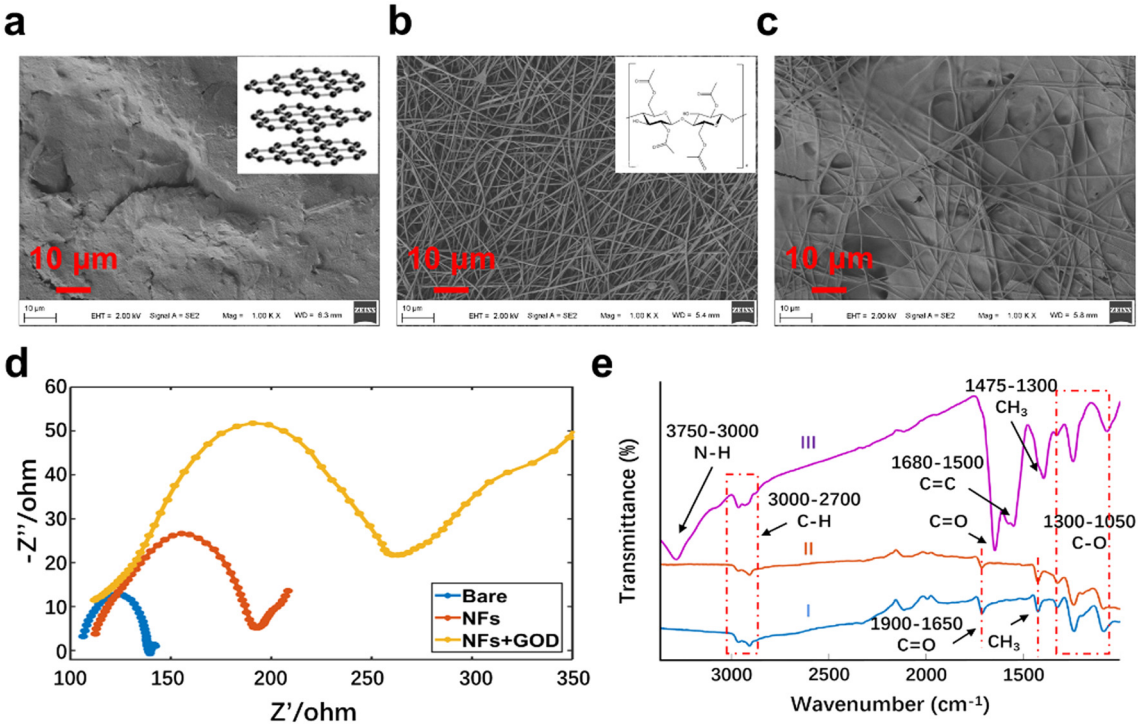

Fig. 3 SEM images of the (a) bare PBSP electrode, (b) CA NF-decorated, and (c) GOD/CA NF-decorated PBSP electrodes; (d) EIS spectrum (blue, red, and yellow lines represent bare, CA NF-decorated, and GOD/CA NF-PBSP electrodes, respectively). (e) FT-IR spectrum ((I) the CA NF-decorated PBSP electrode, (II) the CA NF-decorated PBSP electrodes after the surface treatments, and (III) after the immobilization of GOD onto the CA NF-decorated PBSP electrodes).

Fig. 3e. In curves (I) and (II), characteristic bands were visible at 3000–2700, 1900–1650, 1475–1300, and 1300–1050 cm^{-1}, respectively. The bands at 3000–2700, 1900–1650, 1475–1300, and 1300–1050 cm^{-1} corresponded to the C–H, carbonyl group (C═O), methyl group (–CH_3), and –C–O–, respectively. Fig. 3e (curve III) shows the spectrum after the immobilization of GOD onto the CA NF-decorated PBSP electrodes. Generally, IR bands involved in proton donation and proton acceptance will show shifts toward low energy upon H-bond formation.[36] After the action of EDC and NHS, the C═O bond of CA shows the potential of forming H-bonds with the terminal amine (NH_2) of GOD. The curve (III) showed that the characteristic band at 1712 cm^{-1} shifted toward 1650 cm^{-1}, which is caused by the interaction between the C═O of the CA NF-decorated PBSP electrodes and the amine of GOD.[37] Furthermore, the band at 1300–1050 cm^{-1} was not shifted. The band at 3284 cm^{-1} corresponds to N–H in curve (III). The results show that biomolecules were successfully immobilized onto the surface of CA NF-decorated PBSP electrodes.

3.3 Electrochemical sensing of glucose

Glucose level measurement is one of the most important methods for monitoring diabetes. The results of glucose detection by CA NF-decorated PBSP sensors are shown in Fig. 4a. The DPV curves showed that the peak current increased gradually with the increase in glucose concentration. Compared with the bare PBSP electrode (Fig. S5,† R^2 = 0.77), the peak currents of the CA NF-decorated PBSP electrode for the detection of glucose were linearly associated with concentration, with a linear range from 1 nmol mL^{-1} to 100 μmol mL^{-1} (Fig. 4b, R^2 = 0.96). Similar results were obtained for CV curves (Fig. S6†). Compared with bare PBSP electrodes, CA NF-decorated PBSP electrodes had obvious redox peaks in the CV curve of glucose detection, and the peak current was linearly related to the glucose concentration (R^2 = 0.93). The electrospun CA NF-decorated PBSP electrodes have good biocompatibility, high porosity and hydrophilicity, which increase the binding sites of the antibody in the sensor detection area, allowing the solution to be tested to fully contact the sensor, so it has higher sensitivity. The LOD of the CA NF-decorated PBSP electrode for glucose was 0.71 nmol mL^{-1}, as calculated by three standard deviations of the blank sample. The detection time for each group was ~5 min. The results showed that CA NF-decorated PBSP electrodes had higher detection sensitivity and a wider detection range for glucose.

Moreover, the CA NF-decorated PBSP electrode had good stability (Fig. 4c) and repeatability (Fig. 4d). After the CA NF-decorated PBSP electrodes were stored under an air atmosphere of a normal room at room temperature for 30 days, the electrochemical response remained at 98% of the initial value without being greatly affected. It is proved that the CA NF-decorated PBSP electrode has good stability. However, the electrochemical response of the CA NF-decorated PBSP electrodes modified with GO*x* decreased to about 43% after being stored under the same conditions for 30 days (Fig. S7†). It is speculated that the main reason is that when exposed to air at room temperature, the activity of the enzyme gradually decreases, and the catalytic ability also decreases, thus affecting the

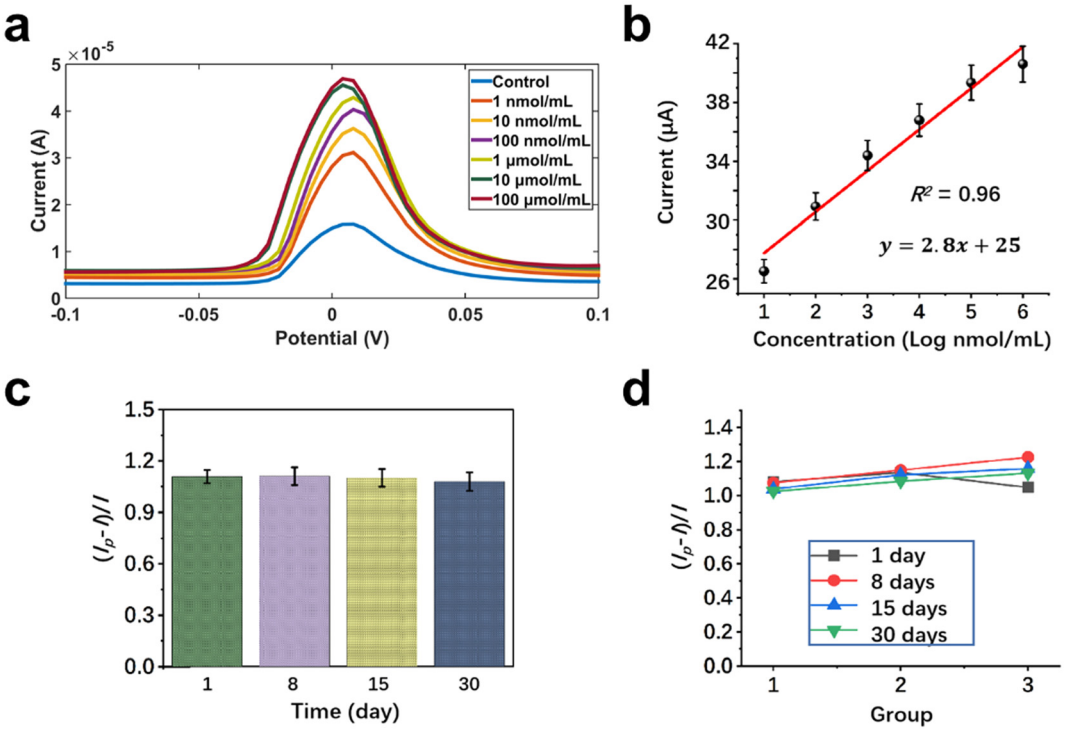

Fig. 4 General performance of the CA NF-decorated PBSP sensor in detecting glucose. (a) DPV curves and (b) the calibration curve; (c) stability evaluation of the sensor; (d) repeatability test of the sensor (n = 3).

electrochemical response of the CA NF-decorated PBSP electrodes. The reproducibility of the CA NF-decorated PBSP electrodes was also analyzed, and the deviation between the electrochemical response changes of electrodes prepared in the same batch was less than 8%, indicating that the electrodes have good reproducibility (Fig. 4d). Compared with other electrochemical sensors (Table S1†), the CA NF-decorated PBSP sensor can detect glucose in a wider range of glucose concentrations (1 nmol mL^{-1} to 100 μmol mL^{-1}) and with a lower LOD (0.71 nmol mL^{-1}).

3.4 Electrochemical sensing of the Ag85B protein

CA NF-decorated PBSP electrodes were used to detect the Ag85B protein, and the results are shown in Fig. 5. The Ag85B protein was detected using chronoamperometry (*I–t* curves) with a detection time of 400 s to ensure that the specific interaction between the Ag85B antibody and the protein was complete. Fig. 5a shows that the response current increased as the Ag85B protein concentration increased. A linear correlation (Fig. 5b) was observed between the variation in the response current and the concentration of the Ag85B protein (R^2 = 0.94). The linear detection range of protein concentrations was 100 fg mL^{-1}–10 μg mL^{-1}, and the LOD of the CA NF-decorated PBSP electrode was 89.1 fg mL^{-1}. Compared with bare PBSP electrodes (Fig. S8†), the CA NF-decorated PBSP electrodes had better detection ability for the Ag85B protein.

Subsequently, the specificity of the CA NF-decorated PBSP electrodes was tested. After modifying the Ag85B antibody in the detection region of the CA NF-decorated PBSP electrodes, the recombinant proteins of MTB Ag85B, Ag85A, Ag85C, ESAT6, CFP10 and Mpt64 were tested separately, among which the Ag85B protein specifically bound to the Ag85B antibody and had a high electrochemical response, ~4–10 times that of the others ($p < 0.01$, $N = 3$). The results showed that the CA NF-decorated PBSP sensors demonstrated good specificity. The detection results of proteins by different electrochemical sensors were compared, as shown in Table S2.† The results show that the CA NF-decorated PBSP sensor has more advantages in the detection range and sensitivity of the protein.

3.5 Electrochemical sensing of *E. coli O157:H7*

E. coli O157:H7 is a kind of *Escherichia coli* bacterium that can cause hemorrhagic diarrhea and enteritis in humans. The chronoamperometry technique (*I–t* curves) was also used for electrochemical sensing of *E. coli O157:H7*. Fig. 6 shows the results of *E. coli O157:H7* detection using the CA NF-decorated PBSP electrodes modified with the *E. coli O157:H7* monoclonal antibody. Fig. 6a shows that the response current increased as the concentrations of *E. coli O157:H7* at 1.5 × 10^2–1.5 × 10^6 CFU mL^{-1} increased. A linear correlation was observed between the variation in the response current and the concentration of *E. coli O157:H7*, with an LOD of 30 CFU mL^{-1} (R^2 = 0.97; Fig. 6b). However, the CA NF-decorated PBSP electrodes without the *E. coli O157:H7* monoclonal antibody did not respond significantly to different concentrations of *E. coli O157:H7* (Fig. S9†). This also showed that the *E. coli O157:H7* monoclonal antibody was successfully immobilized on the surface of the CA NF-decorated PBSP electrodes. The detection of *E. coli O157:H7*, *E. coli ATCC8099*, and *Bacillus subtilis ATCC9372* showed that the CA NF-decorated PBSP electrodes modified with the *E. coli O157:H7* monoclonal antibody demonstrated good specificity (Fig. 6c). The bacterial detection performance of different electrochemical sensors was com-

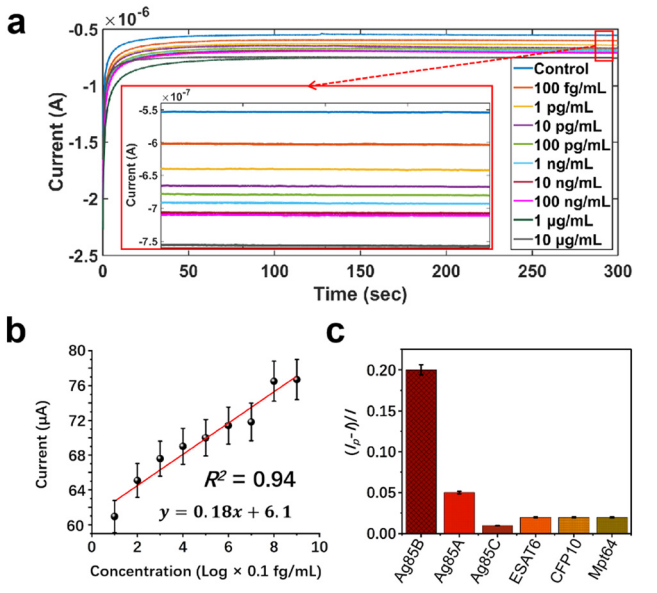

Fig. 5 Performance of the CA NF-decorated PBSP sensor in detecting protein. (a) *I–t* curves and (b) the calibration curve of Ag85B protein detection; (c) specificity evaluation of Ag85B protein detection.

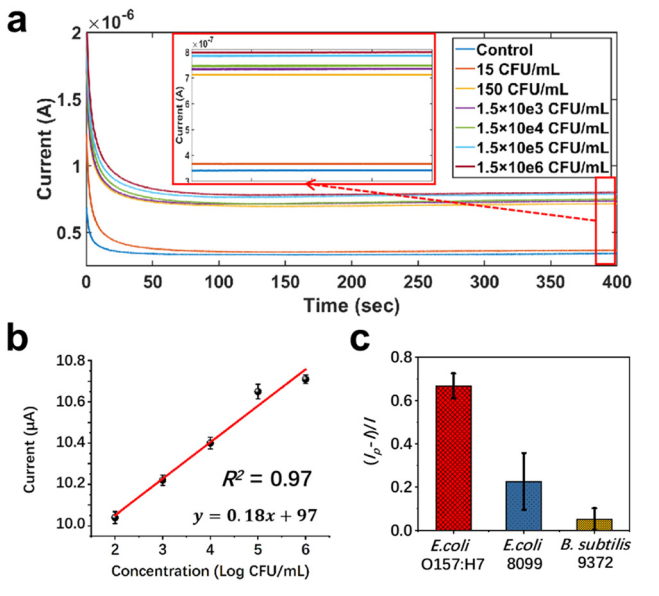

Fig. 6 Performance of the CA NF-decorated PBSP sensor in detecting bacteria. (a) *I–t* curves and (b) the calibration curve of *E. Coli O157:H7* detection; (c) specificity evaluation (compared with *E. coli ATCC8099* and *Bacillus subtilis ATCC9372*).

pared, as shown in Table S3.† In comparison with the other sensors, the CA NF-decorated PBSP sensor showed higher sensitivity for the detection of bacteria.

4 Conclusion

In this study, we designed a simple, inexpensive, and disposable CA NF-decorated paper-based electrochemical biosensor to detect glucose, Ag85B protein, and *E. coli O157:H7*. The electrospun CA NFs were directly bonded to the PBSP electrode using a simple electrospinning technique. Typical electrochemical sensing methods including CV, DPV, and chronoamperometry were used to evaluate the CA NF-decorated PBSP sensor's performance. The fabricated CA NF-decorated PBSP sensor exhibited a short detection duration of ~5–7 min and a detection range of 1 nmol mL^{-1}–100 μmol mL^{-1}, 100 fg mL^{-1}–10 μg mL^{-1}, and 1.5×10^2–10^6 CFU mL^{-1} for glucose, Ag85B protein, and *E. coli O157:H7*, respectively. In addition, the CA NF-decorated PBSP electrode had good stability, reproducibility, and specificity. In summary, the electrospun CA NF decoration remarkably enhanced the detection performance of the PBSP electrodes, and the CA NF-decorated PBSP electrode can be used for typical electrochemical tests as a general electrochemical sensor. These CA NF-decorated PBSP electrodes can detect organic substances, proteins, and bacteria and are expected to achieve the POCT of pathogenic microorganisms and have wide application prospects in biomedicine, clinical diagnosis, environmental monitoring, food safety, and other fields.

Conflicts of interest

There are no conflicts to declare.

References

1 E. Cesewski and B. N. Johnson, *Biosens. Bioelectron.*, 2020, **159**, 112214.
2 J. Ma, M. Du, C. Wang, X. Xie, H. Wang, T. Li, S. Chen, L. Zhang, S. Mao, X. Zhou and M. Wu, *ACS Sens.*, 2021, **6**, 3367–3376.
3 A. Rani, V. B. Ravindran, A. Surapaneni, N. Mantri and A. S. Ball, *Int. J. Food Microbiol.*, 2021, **349**, 109233.
4 J. Wang, *Chem. Rev.*, 2008, **108**(2), 814–825.
5 H. Jadari, M. Amiri, E. Abdi, S. L. Navid, J. Bouckaert, R. Jijie, R. Boukherroub and S. Szunerits, *Biosens. Bioelectron.*, 2021, **124–125**, 161–166.
6 S. H. Baek, M. W. Kim, C. Y. Park, C. Choi, S. K. Kailasa, J. P. Park and T. J. Park, *Biosens. Bioelectron.*, 2019, **139**, 223–229.
7 M. Z. H. Khan, M. R. Hasan, S. I. Hossain, M. S. Ahommed and M. Daizy, *Biosens. Bioelectron.*, 2020, **166**, 112431.
8 V. B. C. Lee, N. F. Mohd-Naim, E. Tamiya and M. U. Ahmed, *Anal. Sci.*, 2018, **34**, 7–18.
9 P. Rajapaksha, A. Elbourne, S. Gangadoo, R. Brown, D. Cozzolino and J. Chapman, *Analyst*, 2019, **144**(2), 396–411.
10 M. Amiri, A. Bezaatpour, H. Jafari, R. Boukherroub and S. Szunerits, *ACS Sens.*, 2018, **3**, 1069–1086.
11 O. Simoska and K. J. Stevenson, *Analyst*, 2019, **144**(22), 6461–6478.
12 J. Xu, C. Cheng, X. R. Li, Y. L. Lu, S. Hu, G. Liu, L. H. Zhu, N. Wang, L. C. Wang, P. Cheng, B. Su and Q. J. Liu, *Biosens. Bioelectron.*, 2021, **185**, 113265.
13 O. Amor-Gutiérrez, E. Costa-Rama and M. T. Fernández-Abedul, *Sensors*, 2022, **22**, 6232–6257.
14 S. Kuss, H. M. Amin and R. G. Compton, *Chem. – Asian J.*, 2018, **13**(19), 2758–2769.
15 M. Amiri, A. Bezaatpour, H. Jafari, R. Boukherroub and S. Szunerits, *ACS Sens.*, 2018, **3**(6), 1069–1086.
16 M. Rastogi and S. K. Singh, in *Defense against Biological Attacks: Volume II*, ed. S. K. Singh and J. H. Kuhn, Springer International Publishing, Cham, 2019, pp. 281–310.
17 D. Grieshaber, R. MacKenzie, J. Voros and E. Reimhult, *Sensors*, 2008, **8**, 1400–1458.
18 A. W. Martinez, S. T. Phillips, G. M. Whitesides and E. Carrilho, *Anal. Chem.*, 2010, **82**, 3–10.
19 C. Zhu, G. Yang, H. Li, D. Du and Y. Lin, *Anal. Chem.*, 2015, **87**, 230–249.
20 S. Smith, K. Goodge, M. Delaney, A. Struzyk, N. Tansey and M. Frey, *Nanomaterials*, 2020, **10**, 2142.
21 X. Li, Q. Feng, K. Lu, J. Huang, Y. Zhang, Y. Hou, H. Qiao, D. Li and Q. Wei, *Biosens. Bioelectron.*, 2021, **171**, 112690.
22 X. Wang, Y. Wang, M. Jiang, Y. Shan, X. Jin, M. Gong and X. Wang, *Anal. Biochem.*, 2018, **548**, 15–22.
23 S. Zhou, M. Hu, X. Huang, N. Zhou, Z. Zhang, M. Wang, Y. Liu and L. He, *Microchim. Acta*, 2020, **187**, 219.
24 M. Gordegir, S. Oz, I. Yezer, M. Buhur, B. Unal and D. O. Demirkol, *Enzyme Microb. Technol.*, 2019, **126**, 24–31.
25 S. A. Zaidi, *Biosensors*, 2021, **11**, 89–96.
26 H. Sun, J. Deng, L. Qiu, X. Fang and H. Peng, *Energy Environ. Sci.*, 2015, **8**, 1139–1159.
27 V. Thavasi, G. Singh and S. Ramakrishna, *Energy Environ. Sci.*, 2008, **1**, 205–221.
28 D. Chauhan and P. R. Solanki, *ACS Appl. Polym. Mater.*, 2019, **1**, 1613–1623.
29 C. Park, J. Lee, D. Lee and J. Jang, *Sens. Actuators, B*, 2022, **355**, 131321.
30 M. S. Ali, K. Mondal, C. Singh, B. D. Malhotra and A. Sharma, *Nanoscale*, 2015, **7**, 7234–7245.
31 Y. Zhai, D. Wang, H. Liu, Y. Zeng, Z. Yin and L. Li, *Anal. Sci.*, 2015, **31**, 793–798.
32 A. Ahmadi, S. M. Khoshfetrat, S. Kabiri, L. Fotouhi, P. S. Dorraji and K. Omidfar, *IEEE Sens. J.*, 2021, **21**, 9210–9217.
33 C. T. Fakude, O. A. A. Arotiba, F. Arduini and N. Mabuba, *Electroanalysis*, 2020, **32**, 1–10.

34 X. Xie, M. Gong, Z. Zhang, X. Dou, W. Zhou, J. Li, M. Zhu, Y. Du and X. Xu, *Sens. Actuators, B*, 2022, **360**, 131432.
35 M. Doostan, H. Maleki, M. Doostan, K. Khoshnevisan, R. Faridi-Majidi and E. Arkan, *Int. J. Biol. Macromol.*, 2021, **168**, 464–473.
36 E. S. Manas, Z. Getahun, W. W. Wright, W. F. DeGrado and J. M. Vanderkooi, *J. Am. Chem. Soc.*, 2000, **122**, 9883–9890.
37 D. Li, G. Li, P. Lv, N. Ullah, C. Wang, Q. Wang, X. Zhang and Q. Wei, *RSC Adv.*, 2015, **5**, 30602–30609.